Cryo-Electron Microscopy Single Particle Reconstruction of Virus Particles using Compressed Sensing Theory

Min Woo Kim[a], Jiyoung Choi[a], Liu Yu[a], Kyung Eun Lee[b], Sung-Sik Han[b], and Jong Chul Ye[a],

[a]Dept. of BioSystems, Korea Advanced Institute of Science and Technology (KAIST)
373-1 Guseong-dong Yuseong-gu, Daejon 305-701, Korea
[b]School of Life Science and Biotechnology, Korea University, Seoul 136-701, Korea

ABSTRACT

Sparse object supports are often encountered in many imaging problems. For such sparse objects, recent theory of compressed sensing tells us that accurate reconstruction of objects are possible even from highly limited number of measurements drastically smaller than the Nyquist sampling limit by solving L_1 minimization problem. This paper employs the compressed sensing theory for cryo-electron microscopy (cryo-EM) single particle reconstruction of virus particles. Cryo-EM single particle reconstruction is a nice application of the compressed sensing theory because of the following reasons: 1) in some cases, due to the difficulty in sample collection, each experiment can obtain micrographs with limited number of virus samples, providing undersampled projection data, and 2) the nucleic acid of a viron is enclosed within capsid composed of a few proteins; hence the support of capsid in 3-D real space is quite sparse. In order to minimize the L_1 cost function derived from compressed sensing, we develop a novel L_1 minimization method based on the *sliding mode* control theory. Experimental results using synthetic and real virus data confirm that the our algorithm provides superior reconstructions of 3-D viral structures compared to the conventional reconstruction algorithms.

Keywords: cryo-EM single particle reconstruction, compressed sensing, sliding mode, iterative shrinkage, L_1 minimization

1. INTRODUCTION

Sparse object supports are often encountered in many biological imaging problems. Classic x-ray crystallography[1] exploits the sparseness of Fourier series coefficients in reciprocal space due to object symmetry. Owing to the sparseness of Fourier series coefficients in reciprocal space, the x-ray crystallography is the only means to achieve the atomic resolution.[1] In icosahedral structural virus reconstruction using cryo-EM, series expansion approaches including the ROSE (Reconstruction by Optimized Series Expansion[2,3]) and EM1[4] also take advantage of the sparsity of series expansion coefficients.

Unlike the sparseness in reciprocal space or expansion coefficients space, sparse support constraint in *real space* has not been fully exploited in either cryo-EM tomography or x-ray crystallography. However, in many cases, imaging objects such as virus particles or microtubule are sparse. Usually, a virus particle is composed of the outer shells (capsid) and the fragile nucleic acid genome.[5] The function of the capsid of a virus particle is to protect the fragile nucleic acid genome from any damages, and to recognize the host cell by binding of a specific virus-attachment protein to a cellular receptor molecule.[5] Therefore, the biologists are interested in the 3-D structure of the thin capsid.

The main purpose of this paper is to fully utilize the sparsity constraint in real space to improve reconstruction quality significantly. Our approach is based on the recent theory in the signal processing community called the *compressed sensing* (CS).[6,7] According to the compressed sensing theory, perfect reconstruction is possible even from the samples dramatically smaller than the Nyquist sampling limit as long as the non-zero spectral support is sparse and the samples are obtained at random.[6,7] Furthermore, an optimal sparse solutions can be obtained by solving an L_1 minimization problem using computationally feasible algorithms such as the basis pursuit,[6–8]

Further author information: (Send correspondence to Jong Chul Ye, Ph.D.)
Jong Chul Ye: E-mail: jong.ye@kaist.ac.kr, Telephone: 82-42-869-4320

Computational Imaging V, edited by Charles A. Bouman, Eric L. Miller, Ilya Pollak
Proc. of SPIE-IS&T Electronic Imaging, SPIE Vol. 6498, 64981G, © 2007 SPIE-IS&T · 0277-786X/07/$18

matching pursuit,[9] iterative soft-thresholding,[10] and etc, rather than resorting to computationally expensive combinatorial optimization algorithm. Hence, the compressed sensing theory has a great potential for imaging problems. The compressed sensing theory nicely fits to the cryo-EM single particle reconstruction because in some experimental condition, only limited number of virus particles can be obtained, providing under-sampled projection data.

As an optimization technique to minimize the L_1 cost function derived from compressed sensing theory, this paper develops a new L_1 minimization method based on *sliding mode* in control theory.[11] Compared to other L_1 minimization such as iterative soft-thresholding,[10] and parallel coordinate descent method (PCD),[12] our algorithm is much stable and less computationally expensive due to the existence of sliding surface. We show that our algorithm is a direct application of *subgradient* based optimization algorithm.[13] We are aware of similar sliding mode based algorithm called the Stablized Inverse DIffusion (SIDE) for image segmentation.[14] However, the application of sliding mode algorithm for L_1 minimization in cryo-EM reconstruction problem is novel. Experimental results using synthetic Bacteriophage PRD1 virus phantoms as well as real Rota virus demonstrate promising reconstruction results.

2. COMPRESSED SENSING FOR SINGLE PARTICLE RECONSTRUCTION

The main contribution of this paper is the development of a novel single particle reconstruction algorithm based on the compressed sensing theory.[6,7] In order to describe the algorithm in detail, we first review the compressed sensing theory.

2.1. Review of Compressed Sensing Theory

Recently, there have been great advance of the compressed sensing theory showing that one can effectively exploit the sparsity or compressibility of an unknown signal in a certain basis to accurately solve severely underdetermined linear inverse problems.[6,7] Specifically, the problem is to solve the following underdetermined inverse problem by measuring K dimensional measurement vector $\mathbf{y} \in \mathbb{C}^K$ from a *linear* mapping:

$$\mathbf{y} = \mathbf{A}\boldsymbol{\rho} \tag{1}$$

where $\boldsymbol{\rho}$ is the N-dimensional unknown vector.* Now, suppose we know *a priori* that the signal $\boldsymbol{\rho} \in \Re^N$ is sparse or compressible in the sense that the re-ordered entries $\rho_{(n)}$ decay like a power-law,

$$|\rho_{(n)}| \leq C \cdot n^{-1/p} \ , \tag{2}$$

for a positive constant C and $0 < p < 1$, where $\rho_{(n)}$ denotes the n-th largest $\boldsymbol{\rho}$ values in discrete domain. Suppose, furthermore, the K by N matrix $\mathbf{A}$ with $K < N$ satisfies certain conditions called CS1-CS3 in.[6] If K discrete measurements are *noisy* and the noise energy is upper-bounded by the input noise power ϵ:

$$||\mathbf{y} - \mathbf{A}\boldsymbol{\rho}||_2 \leq \epsilon \ , \tag{3}$$

then the reconstruction error is bounded above as follows:

$$||\boldsymbol{\rho} - \hat{\boldsymbol{\rho}}_K||_2 \leq C_1\epsilon + C_2(K/\log N)^{-(1/p-1/2)} \tag{4}$$

for some finite constants C_1 and C_2, and $\hat{\boldsymbol{\rho}}_K$ denotes the estimate of $\boldsymbol{\rho}$ from K measurements.[6] Amazing thing about the compressed sensing theory is that the optimal sparse solution satisfying the aforementioned properties can be obtained by solving the L_1 minimization:[6,7]

$$\begin{aligned} &\text{minimize} && ||\boldsymbol{\rho}||_1 \\ &\text{subject to} && ||\mathbf{y} - \mathbf{A}\boldsymbol{\rho}||_2 \leq \epsilon \end{aligned} \tag{5}$$

where $||\cdot||_1$ denote the L_1 norm. It has been shown that the $\mathbf{A}$ matrix in Fourier imaging problem satisfies the CS1-CS3 in.[6] Hence, our goal is to find the computationally efficient but high quality optimization algorithm to address the optimization problem Eq. (5).

*The problem can encompass more general cases where $\boldsymbol{\rho}$ can be represented in a certain orthonormal basis, $\boldsymbol{\rho} = \boldsymbol{\Xi}\boldsymbol{\theta}$, where $\boldsymbol{\theta}$ is the expansion coefficient vector and $\boldsymbol{\Xi}$ denotes the coordinate transform into a certain basis.

2.2. L_1 minimization using Sliding Mode

Direct optimization of Eq. (5) is a difficult task due to the non-differentiable L_1 cost function. Hence, there exist several methods to solve L_1 optimization problem given by Eq. (5). For example, basis pursuit[8] or matching pursuit.[9,15] However, these methods are usually computationally too expensive for 3-D reconstruction problems.

More computationally feasible algorithms have been proposed based on variations of iterative soft-thresholding algorithms.[10,12,16] The $(n+1)$-th estimate of $\boldsymbol{\rho}$ using these algorithms has the following common form:

$$\boldsymbol{\rho}^{(n+1)} = (1-\alpha_n)\boldsymbol{\rho}^{(n)} + \alpha_n \mathcal{S}_{\mathbf{w}_n}\left\{\boldsymbol{\rho}^{(n)} + \mathbf{D}\mathbf{A}^H\left(\mathbf{y} - \mathbf{A}\boldsymbol{\rho}^{(n)}\right)\right\} \tag{6}$$

where the vector soft-thresholding operator $\mathcal{S}_{\hat{\mathbf{w}}}\{\mathbf{z}\}$ is defined by

$$\mathcal{S}_{\hat{\mathbf{w}}}\{\mathbf{z}\} = \begin{pmatrix} \mathcal{S}_{\hat{w}_1}\{z_1\} \\ \mathcal{S}_{\hat{w}_2}\{z_2\} \\ \vdots \\ \mathcal{S}_{\hat{w}_N}\{z_N\} \end{pmatrix}, \quad \mathcal{S}_{\delta}\{z\} = \begin{cases} z-\delta, & \text{if } z \geq \delta; \\ z+\delta, & \text{if } z \leq -\delta; \\ 0, & \text{otherwise.} \end{cases} \tag{7}$$

and the relaxation parameter α_n, the thresholding vector $\mathbf{w}_n \in \Re^N$, and the N by N diagonal weighting matrix $\mathbf{D}$ are dependent on each specific algorithm. Table 1 summarizes how each algorithm uses these parameters.

Algorithm	α_n	$\mathbf{w}_n$	$\mathbf{D}$
Iterative Soft-thresholding[10]	1	$[\lambda, \cdots, \lambda]^T$	$\mathbf{I}^{N\times N}$
Parallel Coordinate Descent[16]	calculated by line search	$\left[\frac{\lambda}{\mathbf{a}_1^H\mathbf{a}_1}, \cdots, \frac{\lambda}{\mathbf{a}_N^H\mathbf{a}_N}\right]^T$	$\left(diag(\mathbf{A}^H\mathbf{A})\right)^{-1}$

Table 1. Comparison of various iterative soft-thresholing algorithms. Here $\mathbf{a}_i$ denotes the i-th column of the $\mathbf{A}$ matrix, $diag(\mathbf{A}^H\mathbf{A})$ is a N by N diagonal matrix composed of the diagonal elements of $\mathbf{A}^H\mathbf{A}$, and $\mathbf{I}^{N\times N}$ denotes the N by N identity matrix, respectively.

Our approach is somewhat different from Eq. (6). Before we discuss our algorithm, let us first review the optimality condition as discussed by Fuchs.[17] Recall that the constrained optimization problem Eq. (5) can be converted into an unconstrained minimization of the following convex cost function

$$\text{QP:} \qquad \min_{\boldsymbol{\rho}}\left\{\frac{1}{2}||\mathbf{y} - \mathbf{A}\boldsymbol{\rho}||_2^2 + \lambda||\boldsymbol{\rho}||_1\right\}, \quad \lambda > 0, \tag{8}$$

where λ denotes the corresponding Lagrangian parameter. Since the QP criterion is nonsmooth at zero, we can introduce a set of vector called the subgradients,[13] denoted $\partial||\boldsymbol{\rho}||_1$:

$$\partial||\boldsymbol{\rho}||_1 = \left\{\mathbf{u} | \mathbf{u}^T\boldsymbol{\rho} = ||\mathbf{x}||_1, ||\mathbf{u}||_\infty \leq 1\right\} \tag{9}$$

$$= \left\{\mathbf{u} \mid \begin{pmatrix} u_i = \text{sign}(\rho_i), & \rho_i \neq 0; \\ |u_i| \leq 1, & \text{otherwise.} \end{pmatrix}\right\} \tag{10}$$

where sign(ρ_i)=1 when $\rho_i > 0$ and sign(ρ_i)=-1 when $\rho_i < 0$. Fuchs[17] showed that the necessary condition (NSC) for $\boldsymbol{\rho}^*$ to be a global minimizer of QP is that the vector zero is a subgradient of the criterion at $\boldsymbol{\rho}^*$:[17]

$$\exists \mathbf{u} \in \partial||\boldsymbol{\rho}||_1 \quad \text{such that} \quad \mathbf{A}^H(\mathbf{A}\boldsymbol{\rho}^* - \mathbf{y}) + \lambda\mathbf{u} = \mathbf{0}. \tag{11}$$

Equivalently, Fuchs[17] showed that the necessary conditions for $\boldsymbol{\rho}^*$ to be a strict minimum of QP can be rephrased as following:

$$\text{NSC1:} \qquad \bar{\mathbf{A}}^H\left(\mathbf{y} - \bar{\mathbf{A}}\bar{\boldsymbol{\rho}}^*\right) = \lambda\text{sign}(\bar{\boldsymbol{\rho}}^*) \tag{12}$$

$$\text{NSC2:} \qquad \left|\mathbf{a}_i^H(\mathbf{y} - \bar{\mathbf{A}}\bar{\boldsymbol{\rho}}^*)\right| \leq \lambda, \quad \text{for all } i = 1, \cdots, N \tag{13}$$

where $\bar{\boldsymbol{\rho}}^*$ and $\bar{\mathbf{A}}$ are the reduced dimensional vector using non-zero components of $\boldsymbol{\rho}^*$ and the corresponding matrix, respectively, such that $\mathbf{A}\boldsymbol{\rho}^* = \bar{\mathbf{A}}\bar{\boldsymbol{\rho}}^*$.

Now, our algorithm is basically sub-gradient based reconstruction algorithm. More specifically, among the various choices of subgradients, at the n-th iteration we choose $\mathbf{g}^{(n)} = [g_1^{(n)}, g_2^{(n)}, \cdots, g_N^{(n)}]^T$:

$$g_i^{(n)} = \begin{cases} -\mathbf{a}_i{}^H \left(\mathbf{y} - \bar{\mathbf{A}}\bar{\boldsymbol{\rho}}^{(n-1)}\right) + \lambda \text{sign}(\rho_i^{(n-1)}), & \rho_i \neq 0; \\ 0, & \text{otherwise.} \end{cases}, \tag{14}$$

because NSC2 guarantees the existence of $|u_i| \leq 1$ for $\rho_i^{(n-1)} = 0$ such that

$$-\mathbf{a}_i^H \left(\mathbf{y} - \bar{\mathbf{A}}\bar{\boldsymbol{\rho}}^{(n-1)}\right) + \lambda u_i = 0 \ . \tag{15}$$

Now, our subgradient search algorithm is to update the estimate using the steepest descent search:

$$\boldsymbol{\rho}^{(n)} = \boldsymbol{\rho}^{(n-1)} - \alpha_n \mathbf{g}^{(n)} \tag{16}$$

where the optimal step size is obtained from line search. It is known that the subgradient algorithm converges to the optimal solution.

However, NSC2 should be satisfied at each iteration to guarantee the convergence of our subgradient algorithm. More specifically, we should have

$$\left|\mathbf{a}_i^H(\mathbf{y} - \mathbf{A}\boldsymbol{\rho}^{(n)})\right| \leq \lambda, \quad \text{for } i = 1, \cdots, N \tag{17}$$

where we again use the equivalence $\mathbf{A}\boldsymbol{\rho}^{(n-1)} = \bar{\mathbf{A}}\bar{\boldsymbol{\rho}}^{(n-1)}$. Eq. (17) can be easily satisfied by choosing sufficiently large λ. Another way is to start with the initial estimate calculated from the minimum norm solution of $\mathbf{y} = \mathbf{A}\boldsymbol{\rho}$:

$$\boldsymbol{\rho}^{(n)} = \mathbf{A}^\dagger \mathbf{y} \tag{18}$$

where $\mathbf{A}^\dagger = \mathbf{A}^H \left(\mathbf{A}\mathbf{A}^H\right)^{-1}$ denotes the pseudo-inverse. For this, we have

$$\mathbf{a}_i^H(\mathbf{y} - \mathbf{A}\boldsymbol{\rho}^{(0)}) = 0 \leq \lambda, \quad \text{for } i = 1, \cdots, N \tag{19}$$

and its subsequent iteration has more chance to satisfy Eq. (17).

It is important to emphasize that our algorithm using Eq. (14) and Eq. (16) has very interesting property that was not observed in other iterative soft-thresholing approach.[10,16] Note that in our algorithm, if $\rho_i^{(n-1)} = 0$, then its subsequent update is also zero, i.e. $\rho_i^{(m)} = 0$ for all $m \geq n$. This implies that the dimension of the state variable or solution $\boldsymbol{\rho}^{(n)}$ is reduced as soon as its elements hit the zero value. This phenomenon is so-called the *sliding mode* in control theory.[11]

More specifically, let us consider an example of 3-D state space trajectory $\boldsymbol{\rho} = [\rho_1, \rho_2, \rho_3]^T$ with a sliding surface as shown in Fig. 1. When a solution trajectory hits the sliding surface (for examples, $\rho_3 = 0$), the consecutive solution trajectory lies in two dimensional state space $\boldsymbol{\rho}^{(m)} = [\rho_1^{(m)}, \rho_2^{(m)}, 0]^T$ for all $m \geq n$. Similarly, if the solution again hits another sliding surface, say $\rho_1 = 0$, the solution trajectory becomes one dimensional. One of the advantages of such state reduction is that the solution is guaranteed to converge in a finite steps.[11] More specifically in our applications, as soon as $\boldsymbol{\rho}_i^{(n)} = 0$, the i-th pixel does not need to recalculated using the back-projection algorithm, or need to be included during the re-projection step. Hence, the overall computational burden can be reduced. Similar sliding mode phenomena was observed in a novel segmentation algorithm called Stablized Inverse DIffusion (SIDE).[14] However, to our knowledge, our sliding mode algorithm for L_1 minimization is novel and has never been used. Note that in discrete implementation there are chances that $\rho_i^{(n)}$ never become zero due to the discrete approximation of the sliding mode. Therefore, we set a small value ϵ, and approximate $\rho_i^{(n)} \simeq 0$ if $|\rho_i^{(n)}| < \epsilon$.

In brief, our algorithm can be summarized as following:

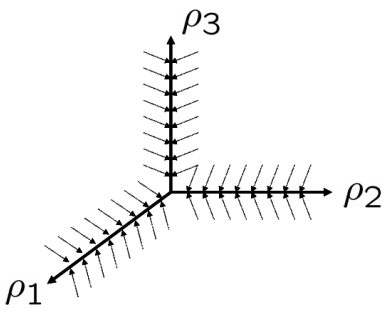

Figure 1. A state space trajectory with sliding surfaces.

- **Initialization.** Set $n = 1$. Choose sufficiently large λ and initialize $\boldsymbol{\rho}^{(0)}$ using the minimum norm solution Eq. (18). Set the non-zero pixel index set $\mathcal{I} = \{1, 2, \cdots, N\}$.
- **Step 1.** Build $\bar{\mathbf{A}}$ and $\bar{\boldsymbol{\rho}}^{(n-1)}$ corresponding the nonzero indexed in $\mathcal{I}$.
- **Step 2.** Calculate subgradient using Eq. (14).
- **Step 3.** Update along the steepest descent direction using Eq. (16).
- **Step 3.** For all $i \in \mathcal{I}$ such that $\rho_i^{(n)} = 0$, remove it from $\mathcal{I}$, i.e. $\mathcal{I} \leftarrow \mathcal{I} \setminus \{i\}$.
- **Step 4.** If $||\mathbf{g}^{(n)}||_2 \leq \epsilon$ for some fixed ϵ, stop it. Otherwise, increase n and go to the Step 1.

3. RESULTS

3.1. Synthetic CCMV Virus

Before dealing with real data, we have tested our algorithm using 3-D synthetic CCMV icosahedral virus data. The synthetic CCMV virus was generated based on shell model using icosahedral harmonics.[18] Synthetic micrograph images are made by projecting the synthetic virus along several view angles. Reconstruction structures was obtained assuming that the view angles are estimated correctly. We use the same projection measurement data set for weighted back-projection (WBP) and our algorithm to have fair comparison. Figs. 3 are reconstruction results by WBP and our algorithm using 100, 500, and 1000 projection views. The reconstructed image resolution gets better with more views, and the WBP results are the worst overall. For the fewer number of views(100-1000 views), the L_1 minimization methods including ours outperforms the gradient methods. Compare to the original slice in Fig. 2(b), CS reconstruction results showed very accurate reconstruction.

The RMS is defined Fig. 5 and calculated. The proposed algorithm converges fastest.

3.2. Real Rota Virus

3.2.1. Experimental Condition

Figs. 6(a)(b) are real Rota virus micrograph data collected using FEI/Philips TECNAI 12 with 120kV. Specifically, Fig. 6(a) are obtained using negative staining, whereas Fig. 6(b) from cryo-TEM. Negative staining clearly shows the details of virus particles in higher resolution; however, such staining procedures destroys the native structures of particles. Hence, Fig. 6(b) are used for our micrograph samples. In Figure 6(b), the particles have no outer layer such as spikes (VP4) and a well-defined rim (VP7) as the morphologic appearance.[5] Therefore, the rota virus particles are not double-shelled but single-shelled virus.[5] Morphology of rota virus is influenced by electron microscope staining procedures (type of stain, PH of stain, and time of staining).[5]

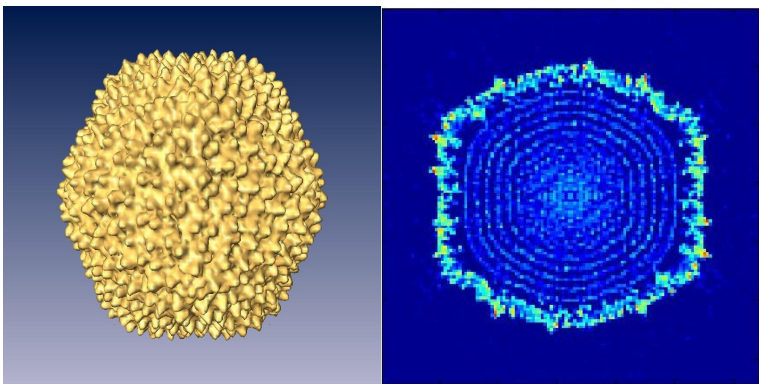

(a) (b)

Figure 2. (a) 3-D structure of Bacteriophage PRD1, and (b) its central slice view.

3.2.2. Image Processing

To reconstruct 3D structure of real rotal virus data, several processing steps are required. Specifically, particles were selected semiautomatically. Total 356 rota virus particles are obtained. For WBP reconstruction, synthetic CCMV virus model is generated and used as a starting model. Then, iterative refinement of an starting 3D model against virus particle images is applied. Specifically, projections of the 3D model are generated with a specified uniform angular sampling distance on the unit sphere taking the icosahedral symmetry into account. Particle images are then classified via measurement of similarity between each raw particle image aligned to each projection image from the model. After the classification, Euler angles are assigned to each virus particles. This view angle estimation process has been already employed in Bsoft.[19] The micrographs and estimated angles are then used for WBP reconstruction to generate the new reference model. This iterative refinement of reference model is performed until it converges. For compressed sensing reconstruction, we use the final WBP reconstruction as a starting model, which is again iterative refined using PCD reconstruction until it converges. The compressed sensing algorithm was implemented by interfacing Bsoft with our routines in MATLAB (Mathworks, Natick, MA).

Figs. (7) are 3-D reconstruction from 356 boxed particles using WBP and CS algorithms, respectively. Surface of 3D structure is visualized by Amira©. Furthermore, during the visualization, our results outperforms others, and it is not sensitive to the thresholding values unlike gradient search. Clearly, in our reconstruction results, the hexahedron structure is more clearly visible with protrusions at each vertex. However, such structure is not clearly in WBP reconstruction. The protein VP6 of rota virus forms the middle layer in the triple-layered viral capsid, and the surface of single-shelled virus depends on the arrangement of VP6 proteins. Our reconstruction structures do not resolve individual VP6. This is due to the low magnification ratio of our experiments.

4. CONCLUSION

This paper employed the compresses sensing theory for high resolution reconstruction of 3-D virus particles from cryo-TEM. Cryo-EM single particle reconstruction of virus was a nice application of the compressed sensing theory because the nucleic acid of a viron is enclosed within capsid composed of a few proteins, hence the support of capsid in 3-D real space is quite sparse. To minimize the L_1 cost function derived from compressed sensing and obtain high resolution three dimensional structure of virus, we develop a novel L_1 minimization method using slide mode. The algorithm iterates between projection, backprojection and shrinkage operation. Furthermore, due to the sliding mode, the dimension of the state variable is continuously reduced when the solution trajectory hits the sliding surface. Experimental results using synthetic and real virus data confirm that the our algorithm provides superior reconstructions of 3-D viral structures compared to the conventional reconstruction algorithms.

5. ACKNOWLEDGEMENT

This work was supported by the Basic Research Program of the Korea Science and Engineering Foundation under Grant R01-2005-000-10035-0. The authors would like to thank Prof. Yibin Zheng at Univ. Virginia for providing the icosahedral harmonics generation routine and CCMV virus parameters.

REFERENCES

1. B. E. Warren, *X-ray Diffraction*, Courier Dover Publications, 1990.
2. R. H. Vogel and S. W. Provencher, "Three-dimensional reconstruction from electron micrographs of disordered specimens. ii. implementation and results," *Ultramicroscopy*, vol. 25, pp. 223–240, 1988.
3. R. H. Vogel, S. W. Provencher, M. Adrian C.-H. Bonsdorff, and J. Dubochet, "Envelope structure of semliki forest virus reconstructed from cryo-electron micrographs," *Nature*, vol. 320, pp. 533–535, 1986.
4. Zhye Yin, Yili Zheng, and P. C. Doerschuk, "An *ab initio* algorithm for low-resolution 3-d reconstructions from cryoelectron microscopy images," *Jour. of Structural Biology*, vol. 133, no. 2/3, pp. 132–142, 2001.
5. T. S. Baker, N. H. Olson, and S. D. Fuller, "Adding the third dimension to virus life cycles: Three-dimensional reconstruction of icosahedral viruses from cryo-electron micrographs," *Microbiology and Molecular Biology Reviews*, vol. 63, no. 4, pp. 862–922, 1999.
6. D. L. Donoho, "Compressed sensing," *IEEE Trans. on Information Theory*, vol. 52, no. 4, pp. 1289–1306, April 2006.
7. E. Candes, J. Romberg, and T. Tao, "Robust uncertainty principles: Exact signal reconstruction from highly incomplete frequency information," *IEEE Trans. on Info. Theory*, vol. 52, no. 2, pp. 489–509, Feb. 2006.
8. S. S. Chen, D. L. Donoho, and M. A. Saunders, "Atomic decomposition by basis pursuit," *SIAM Journal on Scientific computing*, vol. 20, no. 1, pp. 33–61, 1999.
9. J. A. Tropp, "Just relax: convex programming methods for identifying sparse signals in noise," *IEEE Trans. on Information Theory*, vol. 52, no. 3, pp. 1030–1051, March 2006.
10. M.A. Figueiredo and R.D. Nowak, "An EM algorithm for wavelet-based image restoration," *IEEE Trans. on Image Processing*, vol. 12, no. 8, pp. 906–916, August 2003.
11. V. Utkin, J. Guldner, and J. Shi, *Sliding mode control in electromechanical systems*, Systems and Control Series. CRC Press, 1999.
12. M. Elad, B. Matalon, and M. Zibulevsky, "Coordinate and subspace optimization methods for linear least squares with non-quadratic regularization," *submitted*, 2006.
13. R. Fletcher, *Practical Methods of Optimization*, John Wiley & Sons Ltd., England, 2 edition, 1987.
14. I. Pollak, A. S. Willsky, and H. Krim, "Image segmentation and edge enhancement with stabilized inversed-iffusion equations," *IEEE Trans. on Image Processing*, vol. 9, no. 2, pp. 256–266, February 2000.
15. S. G. Mallat and Z. Zhang, "Matching pursuits with time-frequency dictionaries," *IEEE Trans. on Signal Processing*, vol. 41, no. 12, pp. 3397–3415, Dec. 1993.
16. M. Elad, "Why simple shrinkage is still relevant for redundant representations?," *to appear in IEEE Trans. on Info. Theory*, 2006.
17. J. J. Fuchs, "On sparse representations in arbitrary redundant bases," *IEEE Trans. on Information Theory*, vol. 50, no. 6, pp. 1341–1344, June 2004.
18. P.C. Doerschuk and J.E. Johnson, "*Ab Initio* reconstruction and experimental design for cryo electron microscopy," *IEEE Trans. on Info. Theory*, vol. 46, no. 5, pp. 1714–1729, 2000.
19. J. B. Heymann, "Bsoft: Image and molecular processing in electron microscopy," *J. Struct. Biol.*, vol. 133, no. 2/3, pp. 156–169, 2001.

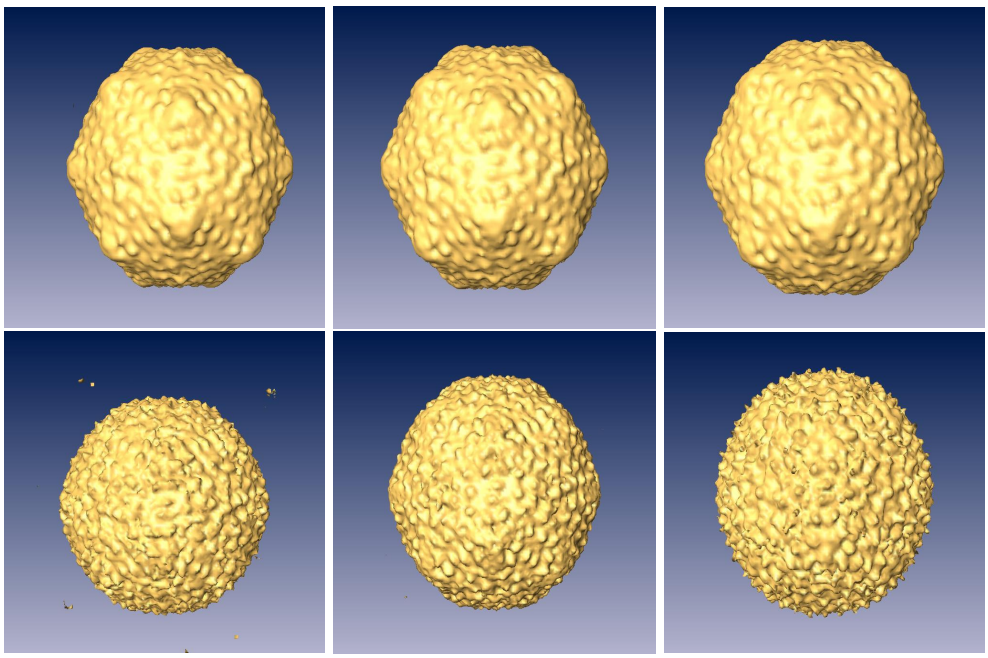

Figure 3. From the left to the right columns: 3-D rendering of Reconstruction using 100, 500 and 1000 projection views, respectively. From the top to the bottom rows: Reconstruction using WBP and our algorithm, respectively .

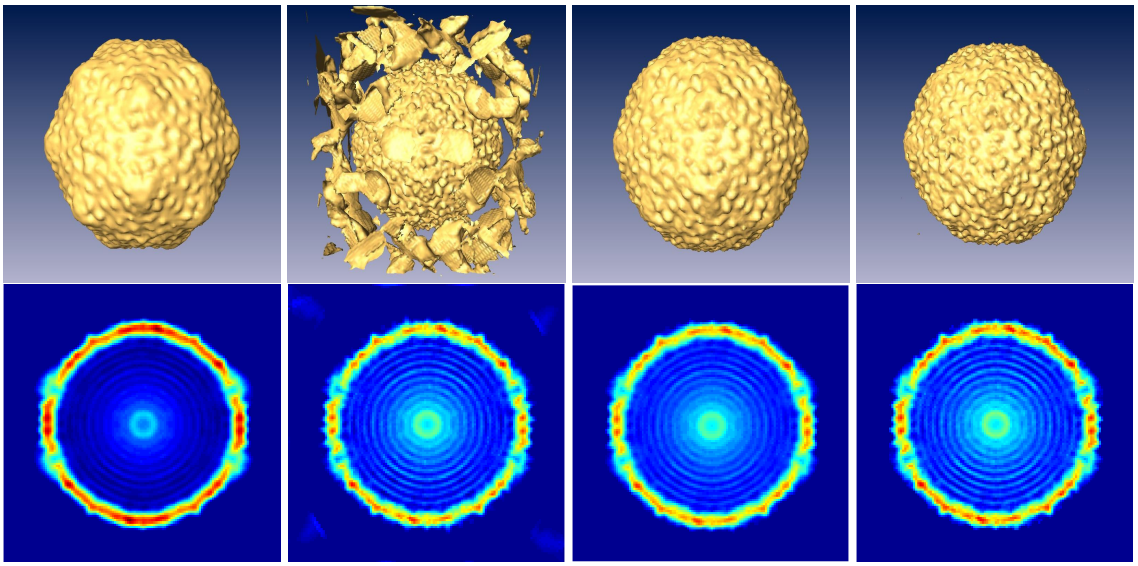

Figure 4. From the left to the right columns: Reconstruction using WBP, steepest descent, iterative soft -thresholding, and the proposed method, respectively. From the top to the bottom rows: 3-D rendering and a central slice, respectively .

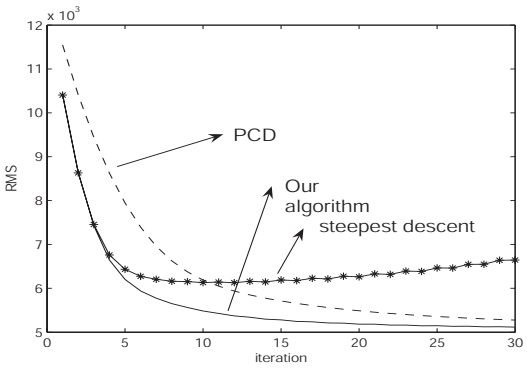

Figure 5. RMS error for the 3-D reconstruction using various algorithms.

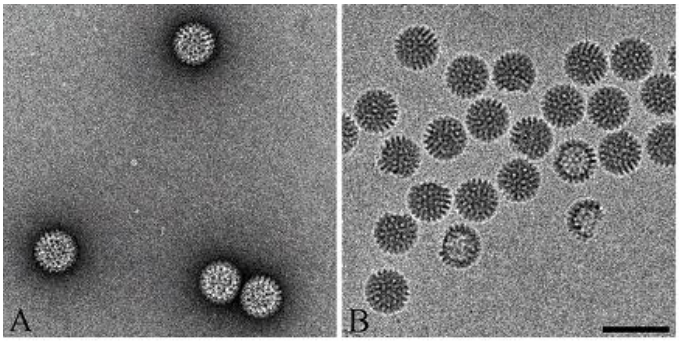

Figure 6. Micrograph of Rota virus collected using FEI/Philips TECNAI12 with 120kV. (a) Negative staining and (b) cryo TEM images.

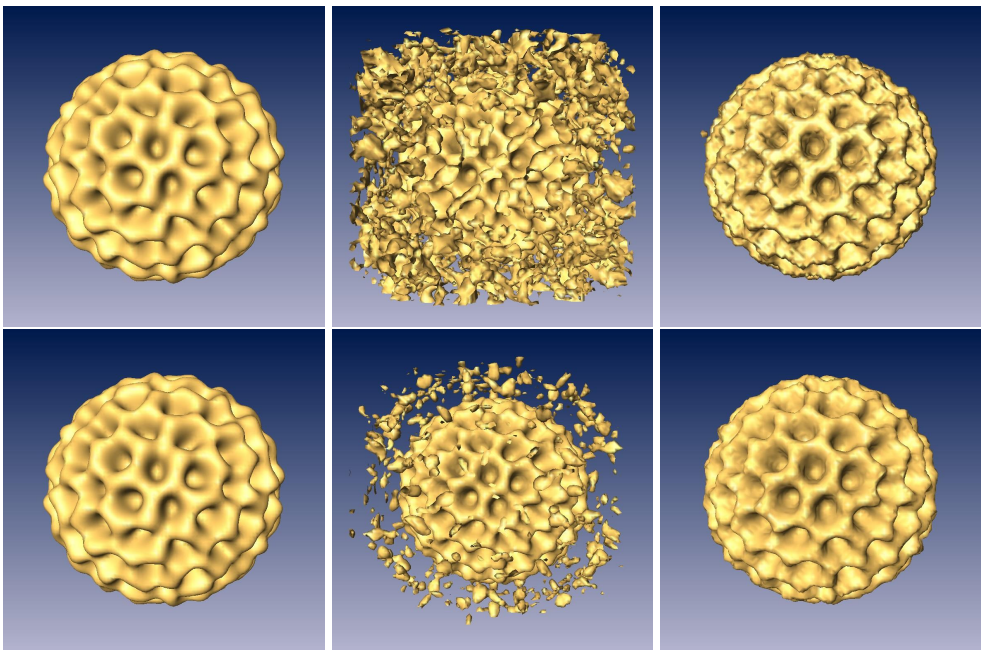

Figure 7. From the left to the right columns: WBP reconstruction, gradient search, and the proposed method, respectively. From the top to the bottom rows: 3-D isosurface at the threshold value of 0.1 and 0.6, respectively .